PAPER

Influence of the impurities in the hybrid discharges with high power in JET ILW

IOP Publishing | International Atomic Energy Agency Nuclear Fusion

Nucl. Fusion **62** (2022) 066010 (9pp) https://doi.org/10.1088/1741-4326/ac2a89

Influence of the impurities in the hybrid discharges with high power in JET ILW

I. Ivanova-Stanik[1,*], C.D. Challis[2], A. Chomiczewska[1], J. Hobirk[3], A. Huber[4], A. Kappatou[3], E. Lerche[5], G. Telesca[1], R. Zagórski[6] and JET Contributors[a]

EUROfusion Consortium, JET, Culham Science Centre, Abingdon, OX14 3DB, United Kingdom
[1] Institute of Plasma Physics and Laser Microfusion, Hery 23, 01-497 Warsaw, Poland
[2] United Kingdom Atomic Energy Authority, Culham Centre for Fusion Energy, Culham Science Centre, Abingdon, Oxon OX14 3DB, UKAbingdon, United Kingdom
[3] Max-Planck Institut für Plasmaphysik Garching, Germany
[4] Forschungszentrum Juelich GmbH, Institut fuer Energie—und Klimaforschung—Plasmaphysik, 52425 Julich, Germany
[5] LPP-ERM/KMS, Association EUROFUSION-Belgian State, TEC partner Brussels, Belgium
[6] National Centre for Nuclear Research (NCBJ), Otwock, Poland

E-mail: irena.ivanova-stanik@ifplm.pl

Received 29 May 2021, revised 15 September 2021
Accepted for publication 27 September 2021
Published 5 April 2022

Abstract

The aim of this paper is to numerically study the influences of the impurities on the high power hybrid discharges in the JET ITER-like wall (ILW) configuration in the DD and deuterium–tritium (DT) scenarios. Numerical simulations with the COREDIV code of hybrid discharges with 32 MW auxiliary heating, 2.2 MA plasma current and 2.8 T toroidal magnetic field in the ILW corner configuration are presented. In the simulations five impurity species are used: intrinsic: beryllium (Be) and nickel (Ni) from the side walls, helium (He) from DT reaction, tungsten (W) from divertor and extrinsic neon (Ne) or argon (Ar) by gas puff. The extrapolation of the DD discharges to DT plasmas at the original input power of 32 MW and taking into account only the thermal component of the alpha-power, does not show any significant difference regarding the power to the target with respect to the DD case. Simulations show that sputtering due to D and T is negligible. In contrast, the simulations at auxiliary heating 39 MW show that the power to the target is possibly too high to be sustained for about 5 s by strike-point sweeping alone without any control by Ne seeding. The tungsten is produced mainly by Ni, Be and seeded impurities.

Keywords: tokamak, JET discharges, integration simulation, impurity

(Some figures may appear in colour only in the online journal)

1. Introduction

The second deuterium–tritium (DT) experimental campaign at the JET ITER-like wall (ILW) (i.e., beryllium first wall and tungsten divertor) is planned in 2021 (JET-DTE2) [1]. The first experiments at JET with 50%/50% DT mixtures were performed in 1997 (DTE1 campaign) [2, 3], where 16 MW of fusion power was achieved transiently and 4 MW in the steady state high power discharges with auxiliary heating (P_{aux}) about 21–26 MW [2]. The operation goal in JET-DT2 is to produce 15 MW fusion power for a 5 s stationary state [4]. Furthermore, DT plasma operation with the ILW has never been attempted in fusion research. In DTE2 campaign discharges are planned at 32 MW of neutral beam injection (NBI) and 6–8 MW of ion cyclotron resonance heating

[*] Author to whom any correspondence should be addressed.
[a] See the author list of 'Overview of JET results for optimising ITER operation' by J. Mailloux *et al* to be published in Nuclear Fusion Special issue: Overview and Summary Papers from the 28th Fusion Energy Conference (Nice, France, 10–15 May 2021).

(ICRH), which represents approximately a factor of 1.5–2 increase in input power with respect to the highest fusion performance plasmas in DTE1. The hybrid scenario development must address connected challenges: first to maintain divertor heat loads within acceptable limits, and second to control the accumulation of the radiative tungsten (W) impurity in the plasma core.

From one side, the seeded impurities can reduce the power to the scrape-off layer (SOL)/divertor regions, due to the increased radiation, leading to reduction of the W influx, but from the other side, they can increase the W production due to enhanced sputtering and could influence the confinement. Therefore, the treatment of both core and the SOL regions together is necessary. Since the energy balance in tokamaks with metallic walls depends strongly on the coupling between bulk and the SOL, plasma integrated modelling approach has to be applied. The COREDIV code is self-consistent with respect to the core–SOL coupling, as well as to impurities-main interaction plasma and in spite of some simplifications, especially in the SOL model (slab geometry and analytical model of the neutrals) the exchange of information between the core (1D) and the SOL (2D) module renders this code quite useful when, as in the case of the JET-ILW, the interaction core–SOL is crucial. In order to assess the plasma parameters in the planned DT experiments COREDIV code [5, 6] has been used to perform integrated simulations of JET DT plasmas. The record shot from the 1997 experiments has been already simulated with COREDIV code and good agreement with experimental data has been found [6].

Numerical simulation for hybrid discharges were done in the past with integrated modelling suite JINTRAC [7], coupling the drift kinetic neoclassical solver NEO [8] and the fast quasilinear gyrokinetic model QuaLiKiz [9]. In such simulation, the W source was used as an input parameter [10]. The numerical analysis with COREDIV code of intrinsic impurity behaviour in neon seeded hybrid discharges with plasma parameters such as the plasma current (I_p), magnetic field (B_T), and NBI were kept the same at 1.4 MA, 1.9 T, and 16.3 MW, respectively are reported in reference [11].

A different trend is observed for mid-Z impurities for the case of Ni where its production comes from structures within the vacuum vessel or is caused by contamination of the plasma facing components. For this reason, the effect of Ne seeding on Ni production should be significantly different compared to W. Additionally, it is worth to add that, e.g., in the case of Ni, its higher release is usually correlated with ICRH heating, while during the presented experiment, only NBI heating was in use. What is also important, results obtained by analysis of the experimental data were consistent with those simulated with the COREDIV code.

In this paper, in order to assess the plasma parameters in the planned DT hybrid discharges results of COREDIV simulations of JET DT plasmas are presented. The aim of this work is investigated of the influence of particles: intrinsic (Ni, Be, He) and extrinsic (Ne, Ar) impurities on the W production, radiation, and power to the plate. Taking the experimental time-average values (about 0.5 s, a few energy confinement times) of total, core radiation, effective charge state and high-Z impurity concentrations and using the steady-state version of the transport code COREDIV we have tried to reconstruct numerically the experimental data.

In section 2 a short description of the COREDIV model is shown, while in section 3 numerical simulations with the COREDIV code of JET hybrid discharge (#92 398) without impurity seeding in the ILW corner configuration are presented. The next step is the extrapolation of the results to DT and TT experiments with auxiliary heating of 32 MW without seeding, which is presented in section 4. In section 5, the influence of Ne and Ar seeding on the main plasma parameters is analysed. Indeed, hybrid experiments have shown a modest impact of Ne seeding at low-mid levels and greater degradation at high levels.

2. The COREDIV model

Simulations were performed using COREDIV code which is based on an integrated approach coupling the radial transport in the core and the 2D multifluid model of the SOL. As this work is a follow-up on our previous calculations the detailed description and parameters used in COREDIV can be found in references [12–15] and only the main points of the model are reported here.

In the core, the 1D radial transport equations for bulk ions, for each ionization state of impurity ions as well as for the electron and ion temperature are solved. We are assuming, that impurity and main plasma ions have the same temperature. We note that important outcome of analysis in reference [16] is that temperature differences between impurity species are always much smaller than between the impurities and hydrogenic species and can usually be neglected. For auxiliary heating parabolic-like deposition profile is assumed and heating due to alpha power is calculated self-consistently taking into account the dilution effect due to helium and impurity transport. The electron and ion energy fluxes are defined by the local transport model proposed in reference [17] which reproduces a prescribed energy confinement law. More precisely the ion and electron conductivities are defined by the formula: $\chi_{e,i}^{an} = C_E \frac{a^2}{\tau_e} \times F(r)$, where a is the minor radius, τ_e is energy confinement time calculated from the scaling law formula (IPB98(y, 2)) in the absence of impurities and the function $F(r)$ describes the parabolic like profile of the conductivity coefficients with a drop near the separatrix due to H-mode barrier formation. In the model we have two options. In one scenario, the parameter C_E is adjusted to keep the calculated confinement time obtained from the solution (without radiation W_{th}/P^{TOTAL}, where W_{th} is thermal energy and P^{TOTAL} is total input power) equal to the value defined by the scaling law. Second option is to fix C_E (and thus $\chi_{e,i}^{an}$) and therefore the confinement will be changed accordingly with changes to the seeding level. By increasing the radiation with impurity seeding, the net heating power decreases, thus when using the first option transport is reduced in order to keep the prescribed confinement. In this case the total plasma energy remains constant together with the energy confinement time. With the second option instead, when transport coefficients are fixed, the total

plasma energy might change. The increased impurity seeding rate always leads to the increase of the net energy confinement time ($W_{th}/(P^{TOTAL} - R^{CORE})$, where R^{CORE} is total radiation power in the core) and the effective τ_p (effective particle residence time) since the power lost into radiation in the plasma core increases.

Some plasmas with low confinement have shown increased H_{98} as seeding was applied. Therefore, in the transport model in COREDIV the two different assumptions are used regarding plasma confinement: (i) constant H_{98} factor or (ii) constant particle and energy transport coefficients (C_E = constant). Indeed, by increasing the core radiation with impurity seeding, the net heating power decreases, thus when using the first option transport is reduced in order to keep the total plasma energy constant. Using second assumption, the confinement will be changed in the code accordingly with changes in the seeding level. The impurity seeding can affect pedestal confinement, as well as core transport and those effects have not been taken into account in this simulation. Indeed, hybrid experiments have shown a modest impact of Ne seeding at low-mid levels and greater degradation at high levels. In other JET discharges with neon seeding rates in the range $\Gamma_{Ne}01.6 \times 10^{21}$ el s^{-1} it was also found that the neon seeding had small effect on the confinement (but it affected the fusion performance due to increasing density and decreasing temperature) [18]. The confinement factor H_{98} has small changes from 1 (without Ne seeding) to 0.94–0.95 for the highest Ne puff level. The question arises of how much this radiation might influence the confinement. For this reason, we have analysed the influence of impurity seeding (Ne, Ar) in the simulations for the case with 39 MW auxiliary heating with two different transport assumptions as explained above.

In the SOL we use the 2D boundary layer code EPIT [19], which is primarily based on Braginskii-like equations for the background plasma and on rate equations for each ionization state of each impurity species. The equations are solved in the simplified slab geometry but taking into account plasma recycling in the divertor and sputtering processes (calculated from [20, 21]) due to all ions: D, T, He, Be, Ni, seeded impurity (Ne, Ar) and W at the target plate. An analytical description of the neutrals is used, that is based on a simple diffusive model. In this model, the effects of the gas puff and of the neutral pumping can be taken into account only by setting up the global recycling coefficient $R = 1 - \Gamma_{SEP}/\Gamma_{PLATE}$, where Γ_{PLATE} is the total particle flux to the target and Γ_{SEP} is the total flux crossing the separatrix. For helium, the recycling was assumed to be ($R_{He} = 2R_H - 1$) in order to keep the helium recycling at a similar level with respect to hydrogen in all simulated cases (note that hydrogen recycling is not constant in our simulations and changes between 0.993 and 0.9965). In the case of Ne seeding a constant value is assumed $R_{Ne} = 0.925$.

In order to keep the prescribed plasma density at the separatrix (at stagnation point), the hydrogen recycling coefficient ($0 < R_H < 1$) was iterated accordingly. The code was run in a steady-state mode neglecting fast phenomena such as, for example, ELMs.

3. Experiment and simulations for DD plasma

In the first step simulations are performed for H-mode hybrid DD discharge #92 398 with 32 MW auxiliary heating, 2.2 MA plasma current and 2.8 T toroidal magnetic field, $H_{98} = 1.3$. This shot executed in 2016 JET campaign has one of the highest fusion performances. In the simulation, five impurities are considered: helium (He) from DT reaction (in the case of DD plasma He is not included), beryllium (Be) from the wall, neon (Ne) puffed in the divertor, nickel (Ni) from fixed source at mid-plane and tungsten (W) self-consistently calculated from sputtering at divertor targets due to all ions. The first source of the nickel particles seen in JET may originate from the remote cutting of some Inconel (58% Ni, 21% Cr, 9% Mo) brackets, which was carried out during the ILW installation [22]. The second source is due to the ion cyclotron range of frequencies antennas, is located in the mid-plane of the vacuum vessel. The application of ICRH usually leads to an overall increase of the plasma impurity content, and in particular W and Ni in JET's ILW [23]. For this reason, in the simulations, the Ni impurity is represented in the simulations as a uniform gas puff from the JET wall.

The auxiliary heating by means of 27 MW of NBI power and 5 MW of ICRH in dipole at 42.5 MHz for H minority heating are used in this shot at the time $t = 7.5$ s. Hybrid shots operates at a lower density and higher $\beta_p(1.0 \div 1.2)$ compared to the alternative baseline scenario $\beta_p(0.5 \div 0.6)$. For this reason, the ratio between ion (T_i) and electron (T_e) temperature (T_i/T_e) measurement in the experiment is higher for hybrids shots ($\sim$1.2–1.3). In the simulation, we assume that most of the input power goes to ions ($P_e^{AUX}/P_i^{AUX} = 0.35/0.65$). This is in agreement with simulations in reference [10] for JET hybrid conditions.

The Ni concentration is calculated from the VUV spectroscopy data (known as the KT2 diagnostic at JET) for a position at the normalized radius 0.5–0.6. The electron temperature for the comparison of experimental and simulated profile in the paper is obtained from the JET high resolution Thomson scattering system HRTS [24]. In figure 1 the experimental and reconstructed electron density, ion and electron temperature, W and Ni concentration core profiles for shot #92 398 time $t = 7.5$ s are shown. The numerical results are compared with experimental data averaged over several ELM periods since production as well as flushing out of W due to individual ELMs are not accounted for in the present steady-state COREDIV model. There is a good agreement between our results and experimental results for total, core and SOL radiation, Z_{EFF} (1.77 in the experiment, 1.72 is the simulation), and W and Ni concentration. The main contributors to increase in Z_{EFF} is nickel and wolfram, which is an effect of the high electron temperature. For normalized radius of 0.5 the dominating ionization state for nickel is Ni^{26+}, but for wolfram is W^{44+}.

Sputtering of W along divertor plate due to different impurities: Be, Ni and W and due to different ionization stages is shown in figure 2 ($d = 0$ m corresponds to the strike point position). Simulations reveal that for Be the sputtering due to Be^{2+} is dominant, which is in agreement with the results

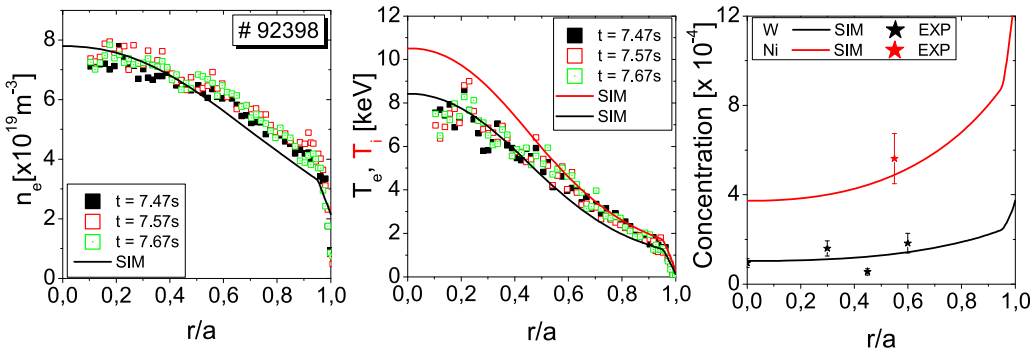

Figure 1. Experimental and simulated electron density, electron (and ion) temperature profiles, W and Ni concentration for #92 398 $t = 7.5$ s.

Table 1. Predictive simulations for DT and TT plasmas at 32 MW. Results for $\Gamma_{\rm Ni} = 1.2 \times 10^{20}$ atm s^{-1} are marked by * in the last two columns.

Parameters	D–D SIM	D–T SIM	T–T SIM	T–T SIM
$P_\alpha^{\rm th}$ (MW)		0.9		
$R^{\rm TOTAL}$ (MW)	11.86	11.84	11.34 (13.08*)	13.5 (15*)
$R^{\rm CORE}$ (MW)	8.7	8.6	8.11 (9.55*)	10.1 (11.35*)
$Z_{\rm EFF}$	1.7	1.72	1.7 (1.9*)	1.85 (2.055*)
$P^{\rm PLATE}$ (MW)	20.14	20.16	20.66 (19*)	18.5 (17*)
$C_{\rm W}$ [$\times 10^{-4}$]	1.55	1.56	1.44 (1.5*)	1.88 (1.9*)
$C_{\rm Be}$ (%)	1	1	1 (1*)	1 (1*)
$C_{\rm He}$ (%)	0	0.11	0 (0*)	4.6 (4.6*)
$C_{\rm Ni}$ [$\times 10^{-4}$]	5.7	5.7	5.8 (9.2*)	5.8 (9.45*)
$W^{\rm sputt}$ by D(T) [$\times 10^{19}$1/s]	0	0	0 (0*)	0 (0*)
$W^{\rm sputt}$ by He [$\times 10^{19}$1/s]	0	0.01	0 (0*)	0.9(0.07*)
$W^{\rm sputt}$ by Be [$\times 10^{19}$1/s]	2.56	2.6	2.5 (2.15*)	2.5 (2.18*)
$W^{\rm sputt}$ by W [$\times 10^{19}$1/s]	4.41	4.6	3.9 (3.6*)	4.6 (4.1*)
$W^{\rm sputt}$ by Ni [$\times 10^{19}$1/s]	2.5	2.5	2.4 (3.14*)	2.18 (2.9*)
$T_{\rm e}^{\rm PLATE}$ (eV)	26.3	26.2	25.1(23.4*)	28.3 (26.3*)

reported in reference [25]. For Ni the largest contribution to the sputtered flux is from Ni^{5+} and Ni^{6+} ionization states, whereas for W the maximum sputtering is caused by W^{6+} ionization state. The sputtering due to W ions have maximum in the strike point and decreases along divertor plate. For Ni and Be we observe more uniform sputtering along plate with maxima shifted away from the strike point.

4. Extrapolation for DT and TT plasma without impurity seeding

In the next step the results are extrapolated to DT and TT keeping unchanged the auxiliary power and the confinement enhancement factor H_{98}. A slight increase in $\tau_{\rm E}$ (due to mass dependence) leads to higher ion and electron temperatures in centre. The ion temperature increases by about 10% for DT plasma and by about 15% for TT case. We note that our simulations are limited to the estimation of the thermal component of the α-power. In the hybrid scenario, since the plasma density is lower and the neutral beams can penetrate better an into the plasma core, the thermonuclear reactions account for ∼35% of the total yield [4]. From our simulation for DT plasma the thermal α-power is 0.96 MW, but if you assume that thermal α-power is only 35% of the total α-power, the resulting total fusion power will be about 13.7 MW. In the simulation for shot #92 398 (corner magnetic configuration) W production by D sputtering is negligible (see table 1). For light ions incident on heavy materials, the sputtering yield depends on the mass and shift of the impact energy threshold to lower value. Extrapolation to DT operation shows no changes in the W concentration and radiation in the core. Tungsten is produced only due to impurities (Be, Ne, Ni) and by self-sputtering. We point out that the temperature at the divertor plate in the strike point is about 25 ÷ 26 eV in simulation, which is lower than T(D) sputtering threshold and consequently sputtering due to D and T is negligible.

The result of a previous analysis of sputtering in JET ILW baseline H-mode plasmas [25], indicated that the W erosion in H-mode plasma is driven by intra-ELM sputtering of W by deuterons as dominant projectile species whereas inter-ELM sputtering by Be ions is either almost absent (inner divertor) or low as 25% (outer divertor) for the given Be concentration of less than 1.0%. This is in contrast with our simulation in which W sputtering is caused by impurities (Be, Ni, Ne) and self-sputtering. First, we note that analysis in reference [25] is done for shots with vertical/semi-horizontal strike-line

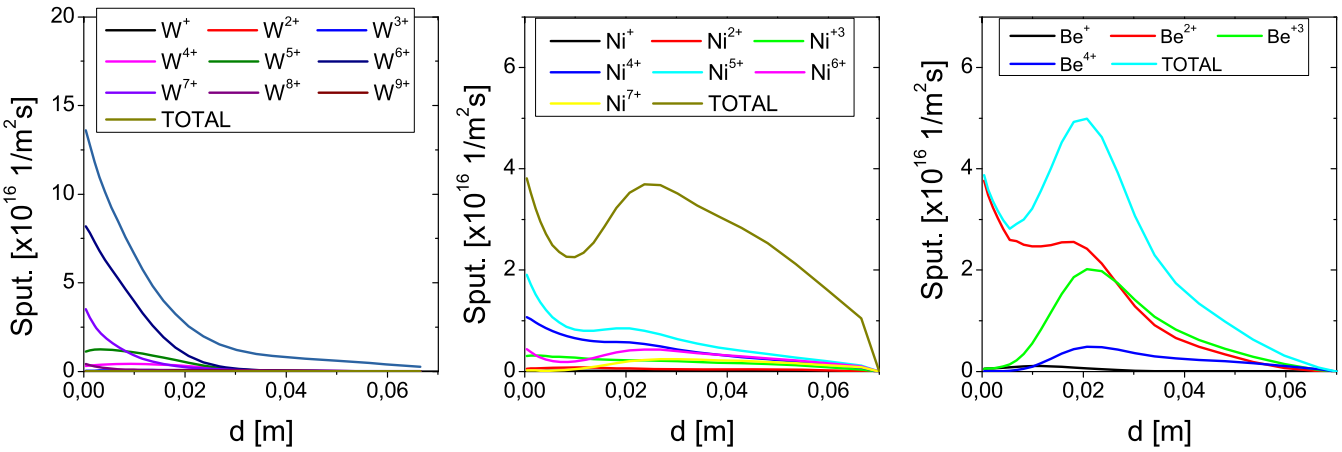

Figure 2. Sputtering along divertor plate for different impurities: Be, Ni and W by different ionisation state.

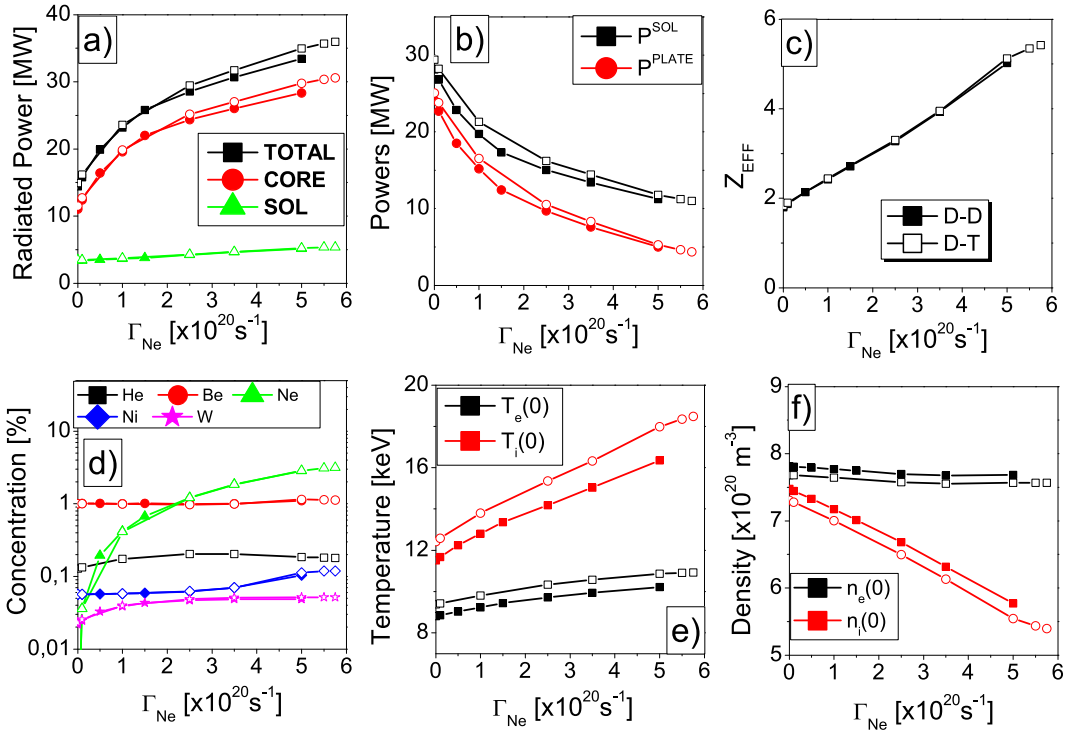

Figure 3. Main code outputs. (*a*) Radiation, (*b*) power to the plate and to SOL, (*c*) effective charge state, (*d*) impurity concentration, (*e*) temperature and (*f*) density in centrum for DD (full symbol) and DT (open symbol) as a function of Ne gas puff level.

configuration (open divertor) characterized by higher edge temperatures whereas, our simulation is for corner configuration (closed divertor). Second, in the experimental shot #92 398 strike point sweeping is used for spreading the heat loads over a larger surface area of plasma facing components which in addition decreases temperature at the plate. Finally, our modelling does not consider ELM's, which my induce some sputtering due to D(T) ions.

For JET hybrid conditions, the simulations in reference [10] predict that ion heating schemes (e.g. He-3 minority, or three-ion schemes) increase neoclassical temperature screening and could be more efficient for central W control. Three scenarios for high magnetic field ($B_T = 3.4$ T) operation were tested and compared: (i) hydrogen minority heating, (ii) ^{3}He minority heating and (iii) the combination of the former two by simultaneous use of two RF frequencies in reference [26]. Whereas the former of these schemes has already proven to have good potential, the second is to be preferred for application in D–T plasmas since ^{3}He minorities can be used to increase the D–T fusion reactivity. For this reason in the case with TT, we have investigated the influence of He to W production. For this aim, we compare the case without and with 4.6%

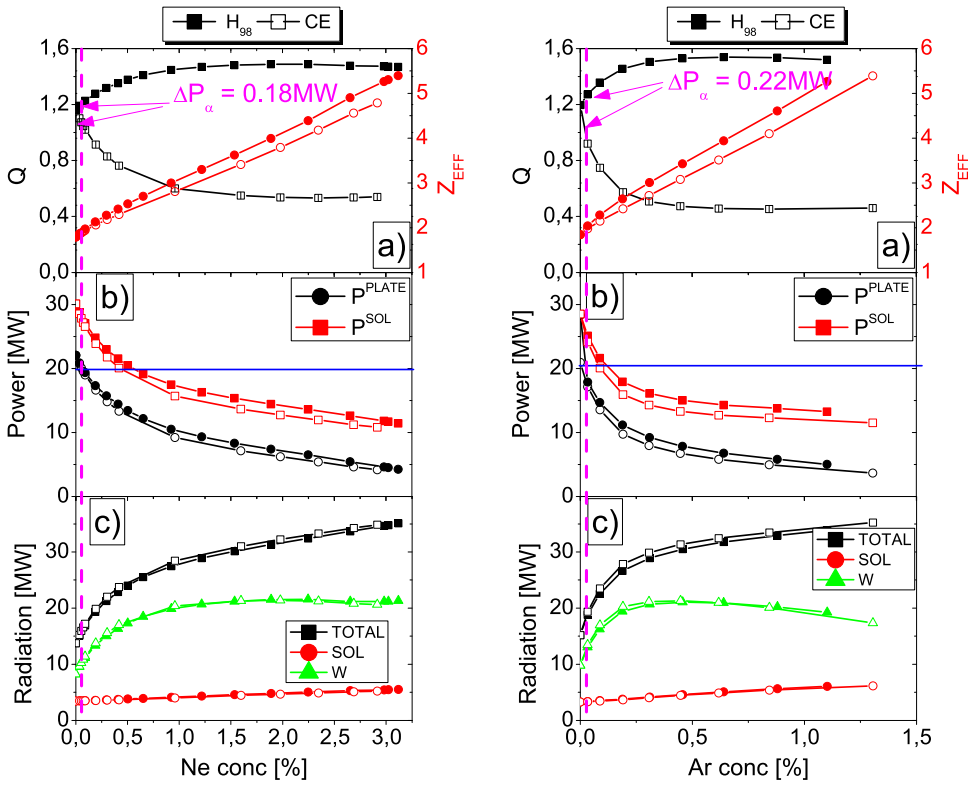

Figure 4. Plasma parameters. (*a*) Q-factor and Z_{EFF}, (*b*) power to the plate and to SOL, (*c*) total, SOL and W radiation, for H_{98} = constant (full symbol) and C_{E} = constant (open symbol) as a function of Ne (left panel) and Ar (right panel) concentration.

He concentration (last two column in table 1). In table 1 the main plasma parameters are reported as: α power by thermal DT reaction (P_{α}^{th}), total (R^{TOTAL}) and core (R^{CORE}) radiation, effective charge (Z_{EFF}), power to the divertor plate (P^{PLATE}), tungsten (C_{W}), beryllium (C_{Be}) and nickel (C_{Ni}) concentration, the averaged sputtering fluxes along the plate by D(T), He, Be, Ni and W (self-sputtering), electron temperature of the divertor plate ($T_{\mathrm{e}}^{\mathrm{PLATE}}$).

The increase of the He concentration to 4.6% leads to the increase of W production by sputtering due to helium. Consequently, the W concentration in core increases from 1.44×10^{-4} to 1.9×10^{-4}. The radiation in the core increases by 20% and Z_{EFF} changes from 1.7 to 1.85. It is observed, that although Ni and Be have different concentrations (C_{Be} 18 times higher), their effect on the W sputtering is similar for the temperature on the plate of about 2 5 eV. Very small differences between DD and DT in the radiation profile for the case of 32 MW auxiliary heating are observed in the simulations.

The analysis for shot #98 369 (H), #95 645(D) and #98 583 (T) plasma show increase in Ni concentration with increasing atomic number of the main ions. Simulations for TT plasma with higher Ni puff ($\Gamma_{\mathrm{Ni}} = 1.2 \times 10^{20}$ atm s^{-1}) are marked by * in the last two columns of table 1. Comparing the cases with lower and higher Ni puff, we observe small increase in W concentration (C_{W}), total radiation increases by about 1.5 MW, which is the consequence of the increase of the Ni radiation.

5. Extrapolation to DT plasma with Ne and Ar impurity seeding

Our next step for analysis is the extrapolation of the results for DT experiments with auxiliary heating of 32 MW and 39 MW. Nowadays, strike point sweeping is routinely used at JET to spread the heat load over a larger area of the divertor. This method was also used in the shot #92 398. For the 40 MW extrapolation cases with radiation 10–13 MW, the results [27] indicate that a sweeping amplitude between 5.0–6.0 cm on tile 6 would be required to stay within the tile temperature limit for a 5 s pulse and it may just be possible to execute the pulse without having to introduce additional heat load mitigation, e.g., by impurity seeding. The main side effect of sweeping observed in the plasma is modulation of the ELM frequency. With higher frequency 20 Hz sweeping, it was found that the ELMs could become strongly synchronized with the sweeping, although it is not yet clear what are the necessary conditions for this behaviour, and whether it could be an advantage or disadvantage to the scenario. A control of the ELM frequency is beneficial and can play an important role in preventing contamination of the plasma by W in metallic-wall devices [28]. We note that part from their relevance to the issue of W sputtering, ELMs can also act to spread the heat loads in the divertor, in addition to the effect of sweeping. For 39 MW auxiliary heating, recalling that in our simulations only P_{α} arising from thermal reactions is accounted for, the simulations indicate that radiation is 13.7 MW without impurity seed-

ing, which gives radiation fraction about ∼35%. Neon is now often introduced in trace amounts (∼0.2%) for the purpose of improving the ion temperature measurements from charge exchange spectroscopy [16]. Power to the divertor plate is about 26 MW.

For this reason, simulations are performed for seeding with two noble gasses: Ne and Ar for reduced power to the divertor plate. The comparison of the main plasma parameters for both mixtures DD and DT in the case with Ne puff are presented in figure 3.

It can be seen that there are no large differences in radiations, effective charge state, power to the plate, impurity concentrations between both plasma mixtures. Regarding α-power, COREDIV simulations predict an increase in the thermal P_α level at higher Ne seeding rate because of the increase in the main ion temperature, which is dependent on the main ion dilution (see figures 3(*e*) and (f)). Already small amount of Ne puff ($\Gamma_{Ne} \geqslant 0.8 \times 10^{20}$ s^{-1}) leads to significant plasma radiation figure 3(*a*) and reduction of the ELM-averaged power to the divertor figure 3(*b*). With the increase in the Ne seeding level a strong increase of the radiation is observed, the highest level is three times higher. The Z_{EFF} increases almost linearly with the Ne puff level (please note that in our model the same temperature is assumed for all ions) (figure 3(*c*)).

A question arises, how much of this radiation might influence the confinement. For this reason, we have analysed the influence of impurity seeding (Ne, Ar) in the simulations for the case with 39 MW auxiliary heating with two different transport assumptions: first-constant H_{98} factor and second constant particle transport coefficients (C_E = constant). In the figure 4, we show Q-factor, Z_{EFF}, power to the plate and to the SOL, effective charge for both transport schemas as a function of Ne and Ar concentration. In the case where H_{98} is constant, we observe increase in the ion temperature with increasing impurity puff. This has positive effect on the alpha (fusion) production, which increases from 0.96 (4.8) MW to 1.5 (7.5) MW for Ne case. The Ne and Ar seeding are effective in reducing the power to the plate to 5 MW, but steep degradation of the plasma confinement for Ar seeding is observed in the simulations. The vertical line (magenta colour) shows the case when power to the plate is 20 MW. Higher Z_{EFF} for constant H_{98} is the effect of high temperature in core. We remark that difference in P_α between both transport schemas is smaller for Ne puff (0.18 MW). For the case with transport scheme C_E = const, when the power to plate is 20 MW, H_{98} is lower by about 0.08 and 0.12 for Ne and Ar puff, respectively. For Ar seeding, the W concentration increases faster with increasing seeding rate then in the case with Ne seeding.

In the figures 5 and 6 the ion plasma density in core and the ratio between core (R^{CORE}) and SOL (R^{SOL}) radiation for Ar and Ne seeding for both transport schemes are presented. A smaller dilution for both assumptions for the case with Ar seeding is observed. The main ion dilution for constant C_E is smaller than for constant H_{98}, which is the effect of lower temperature. The R^{CORE}/R^{SOL} is higher for the case with Ar seeding in comparison to case with Ne seeding when $P^{PLATE} > 7.5$ MW.

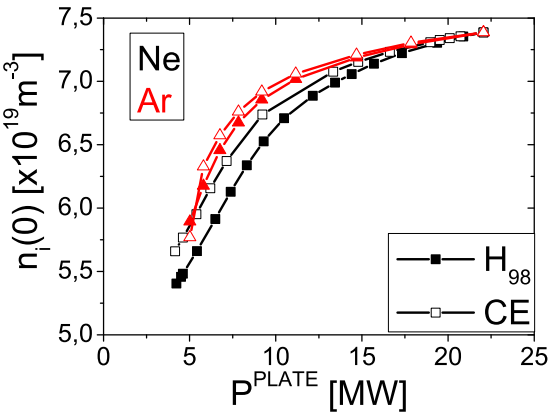

Figure 5. Ion density in plasma centre for Ne and Ar seeding for both transport scheme.

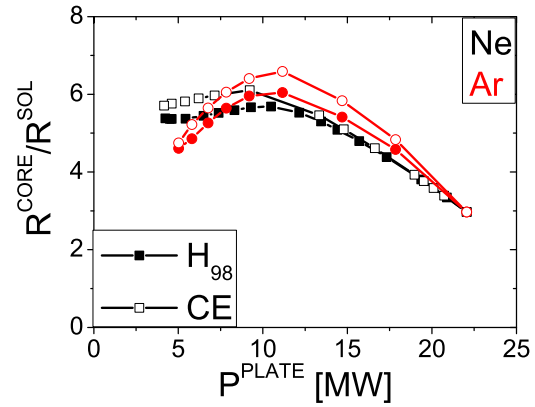

Figure 6. The R^{CORE}/R^{SOL} for Ar and Ne seeding for both transport scheme.

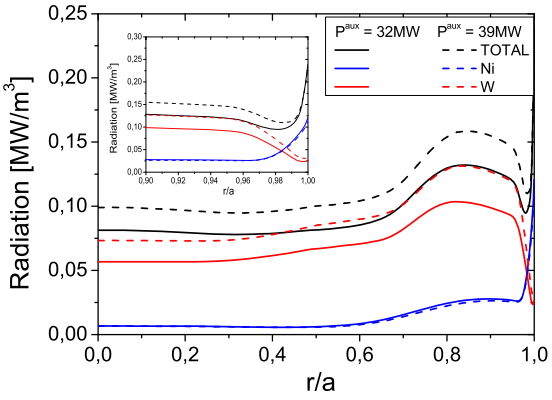

Figure 7. Profile of the core radiation for case with constant H_{98} for two different auxiliary heating values $P^{AUX} = 32$ MW (solid line) and $P^{AUX} = 39$ MW (dash line).

We should note, that with the increase of the heating power to 39 MW, the plasma temperatures increase in the core. As an effect of this the maximum of the radiation shifts towards the pedestal for case with constant H_{98} higher radiation in the pedestal is observed (see figure 7).

6. Conclusions

In order to assess the plasma parameters in the planned JET DT experiments, COREDIV code has been used to perform self-consistent core-edge simulations of DT and TT plasmas. The extrapolation of the DD discharges to DT plasmas at the original auxiliary heating of 32 MW and taking in the account only thermal components of the alpha-power does not show any significant difference regarding the main plasma parameters: power to the target, radiation, effective charge state with respect to the DD case. The simulations show that sputtering of W due to D and T is negligible. For beryllium ions, the dominant contribution to W sputtering is due to Be^{2+}. For Ni and W the largest production of the sputtered fluxes is from ionization states Ni^{5+} and Ni^{6+}, and W^{6+}, respectively. The sputtering due to W is mainly in the strike point, but for Ni and Be is more uniform along the divertor plate. The extrapolation to higher auxiliary heating and DT operation shows decisive influence of the power on plasma parameters: an increase in the W concentration and radiation in the core by about 25%. Tungsten is produced only due to impurities (Be, Ne, Ni)+ self-sputtering. The extrapolation to DT plasmas, with unchanged input power, leads to little difference with respect to the reconstructed DD pulses, using only thermal alpha-power. In the case with Ar seeding lower plasma confinement is predicted.

Acknowledgments

This work has been carried out within the framework of the EUROfusion Consortium and has received funding from the Euratom research and training programme 2014–2018 and 2019–2020 under Grant Agreement No. 633053. The views and opinions expressed herein do not necessarily reflect those of the European Commission. This scientific work was partly supported by the Polish Ministry of Science and Higher Education within the framework of the scientific financial resources in the year 2020 allocated for the realization of the international co-financed Project Nos. 5118/H2020/EURATOM/2020/2 and 5119/H2020/EURATOM/2020/2.

ORCID iDs

I. Ivanova-Stanik https://orcid.org/0000-0002-2766-8612
J. Hobirk https://orcid.org/0000-0001-6605-0068
A. Huber https://orcid.org/0000-0002-3558-8129
A. Kappatou https://orcid.org/0000-0003-3341-1909

References

[1] Joffrin E. *et al* 2019 Overview of the JET preparation for deuterium–tritium operation with the ITER like-wall *Nucl. Fusion* **59** 112021
[2] Keilhacker M. *et al* 1999 High fusion performance from deuterium–tritium plasmas in JET *Nucl. Fusion* **39** 209
[3] Jacquinot J. *et al* 1999 Overview of ITER physics deuterium–tritium experiments in JET *Nucl. Fusion* **39** 235
[4] Garzotti L. *et al* 2019 Scenario development for D–T operation at JET *Nucl. Fusion* **59** 076037
[5] Telesca G. *et al* 2019 COREDIV numerical simulation of high neutron rate JET-ILW DD pulses in view of extension to JET-ILW DT experiments *Nucl. Fusion* **59** 056026
[6] Zagórski R. *et al* 2018 Modelling of JET DT experiments in ILW configurations *Contrib. Plasma Phys.* **58** 739–45
[7] Cenacchi G. and Taroni A. 1988 JETTO: a free-boundary plasma transport code (basic version) *JET Intern. Report JET-IR* **88** 3
[8] Belli E.A. and Candy J. 2008 Kinetic calculation of neoclassical transport including self-consistent electron and impurity dynamics *Plasma Phys. Control. Fusion* **50** 095010
[9] Bourdelle C., Citrin J., Baiocchi B., Casati A., Cottier P., Garbet X. and Imbeaux F. 2016 Core turbulent transport in tokamak plasmas: bridging theory and experiment with QuaLiKiz *Plasma Phys. Control. Fusion* **58** 014036
[10] Casson F.J. *et al* 2020 Predictive multi-channel flux-driven modelling to optimise ICRH tungsten control and fusion performance in JET *Nucl. Fusion* **60** 066029
[11] Krawczyk N. *et al* 2018 Application of the VUV and the soft x-ray systems on JET for the study of intrinsic impurity behavior in neon seeded hybrid discharges *Rev. Sci. Instrum.* **89** 10D131
[12] Zagórski R. *et al* 1996 Numerical modelling of the edge plasma in tokamaks *J. Tech. Phys.* **37** 7–37
[13] Stankiewicz R. *et al* 2001 Self-consistent description of the core and boundary plasma in the high-field ignition experiment *J. Nucl. Mater.* **290–293** 738–42
[14] Stankiewicz R. *et al* 2003 Effect of core-edge coupling on operation regimes of ITER-like reactor *J. Nucl. Mater.* **313–316** 899–903
[15] Telesca G. *et al* 2017 Simulation of JET ITER-like wall pulses at high neon seeding rate *Nucl. Fusion* **57** 126021
[16] Weisen H. *et al* 2020 Analysis of the inter-species power balance in JET plasmas *Nucl. Fusion* **60** 036004
[17] Mandrekas J. and Stacey J.W.M. 1995 An impurity seeded radiative mantle for ITER *Nucl. Fusion* **35** 843
[18] Challiis C.D. *et al* 2017 Impact of neon seeding on fusion performance in JET ILW hybrid plasmas *44th EPS Conf. Controlled Fusion and Plasma Physics* (Belfast, 26–30 June 2017), P2.153 (http://ocs.ciemat.es/EPS2017PAP/pdf/P2.153.pdf)
[19] Zagórski R. 2013 Simulations with the COREDIV code of DEMO discharges *Nucl. Fusion* **53** 073030
[20] Yamamura J. *et al* 1083 Angular dependence o sputtering yields of monatomic solids *Report of the IPP Nagoya IPPJ-AM-26*
[21] Garcia-Rosales G. *et al* 1994 Revised formulae for sputtering data *J. Nucl. Mater.* **218** 8–17
[22] Matthews G.F. 2013 Plasma operation with an all metal first-wall: comparison of an ITER-like wall with a carbon wall in JET *J. Nucl. Mater.* **438** S2–S10
[23] Czarnecka A., Zastrow K.-D., Rzadkiewicz J., Coffey I.H., Lawson K.D. and O'Mullane M.G. 2011 Determination of metal impurity density, ΔZ_{eff} and dilution on JET by VUV emission spectroscopy *Plasma Phys. Control. Fusion* **53** 035009
[24] Pasqualotto R., Nielsen P., Gowers C., Beurskens M., Kempenaars M., Carlstrom T. and Johnson D. 2004 High resolution Thomson scattering for joint European torus (JET) *Rev. Sci. Instrum.* **75** 3891–3
[25] Brezinsek S. *et al* 2019 Erosion, screening, and migration of tungsten in the JET divertor *Nucl. Fusion* **59** 096035

[26] Van Eester D. *et al* 2016 Recent ion cyclotron resonance heating experiments in JET in preparation of a DT campaign *26th IAEA Fusion Energy Conf.* (Kyoto, Japan, 17–22 October) EX/P6-10 (https://nucleus.iaea.org/sites/fusionportal/Shared%20Documents/FEC%202016/fec2016-preprints/preprint0261.pdf)

[27] Silburn S.A. *et al* 2017 Mitigation of divertor heat loads by strike point sweeping in high power JET discharges *Phys. Scr.* **T170** 014040

[28] Dux R., Loarte A., Angioni C., Coster D., Fable E. and Kallenbach A. 2017 The interplay of controlling the power exhaust and the tungsten content in ITER *Nucl. Mater. Energy* **12** 28–35